Original citation:
Gurnani, Pratik, Lunn, Andrew M. and Perrier, Sébastien. (2016) Synthesis of mannosylated and PEGylated nanoparticles via RAFT emulsion polymerisation, and investigation of particle-lectin aggregation using turbidimetric and DLS techniques. Polymer . doi: 10.1016/j.polymer.2016.08.093

Permanent WRAP URL:
http://wrap.warwick.ac.uk/83841

Copyright and reuse:

Publisher's statement:

A note on versions:
The version presented here may differ from the published version or, version of record, if you wish to cite this item you are advised to consult the publisher's version. Please see the 'permanent WRAP url' above for details on accessing the published version and note that access may require a subscription.

For more information, please contact the WRAP Team at: wrap@warwick.ac.uk

warwick.ac.uk/lib-publications

Synthesis of Mannosylated and PEGylated Nanoparticles via RAFT Emulsion Polymerisation, and Investigation of Particle-Lectin Aggregation using Turbidimetric and DLS Techniques

Pratik Gurnani,[a,†] **Andrew M. Lunn,**[a,†] **Sébastien Perrier**[a,b]*

[a]Department of Chemistry, the University of Warwick, Gibbet Hill, Coventry, CV4 7AL, UK
[b]Faculty of Pharmacy and Pharmaceutical Sciences, Monash University, 381 Royal Parade, Parkville, VIC 3052, Australia.

*Corresponding Author: S.Perrier@warwick.ac.uk
[†]These authors contributed equally to this work

Keywords: Colloids, Glyco-polymers, Lectin Binding, Polymer Synthesis, Emulsion Polymerisation

1 **TOC Graphic and Graphical Abstract**

2 **Abstract**:

3 Recent developments in controlled radical polymerisation presents an attractive way of producing

4 biocompatible polymeric nanoparticles for a wide range of applications. With this motivation, well

5 defined P(ManAm) and P(PEGA) coated nanoparticles in a range of different sizes have been

6 synthesised via RAFT emulsion polymerisation. The particles were used to precisely investigate the

7 effect of particle size on lectin binding with Concanavalin A, and validate the use of online DLS

8 measurements for lectin-glycoparticle aggregation studies. Larger particles were found to have an

9 enhanced aggregation by both UV-Vis turbidimetric and DLS aggregation studies. The DLS technique

10 was shown to be robust up to an aggregate diameter of c.500nm for aggregation tests, and was not

11 affected by any dilution or light scattering effects that typically hinder the common use of turbidimetry

12 in particle aggregation studies.

13

14

15 **1. Introduction**

16

17 In the field of drug delivery, targeting of specific cells (e.g. malignant or a bacterial cells) is an

18 important way of delivering therapeutic doses of an active pharmaceutical ingredient (API), whilst

19 minimising its side effects. Targeting cell surface proteins with their complementary ligand is one way

20 of directing an API to its site of action. Lectins are a well-known example of surface protein, expressed

21 by both bacterial and mammalian cells. One of the main properties of lectins is their highly specific

22 ligand-receptor interaction *via* non-covalent bonds with carbohydrates.[1-3] One potential solution for

23 cell targeting, is to harness these non-covalent interactions, with the use of polyvalent saccharide coated

24 'glyconanoparticles' acting as targeted delivery agents. Many glyconanoparticles consist of a metallic

core (e.g. gold) with a glycosylated shell.[4, 5] However, the versatility of polymer chemistry has allowed researchers to modify all aspects of nanoparticle structure such as core/shell composition, shape, size and degradability, which is suited to the synthesis of well-defined glyco-nanoparticles.[6]

Interest in the field of glycosylated nanomaterials has grown rapidly over the previous two decades, particularly for their use as biosensors[3, 7] or targeting agents[8]. However, to fully understand the interactions these materials have within a complex biological system, researchers must look towards model systems which are equivalent in most aspects but instead are inert to unspecific interactions with carbohydrate. Poly(ethylene glycol) is the most widely known 'stealthy' polymer, and is typically used as a coating to avoid protein adsorption and subsequent immune response *in vivo*.[9] This property of PEG is usually attributed to an enhanced hydration effect of the hydrophilic polymer chains resulting in steric hindrance or 'shielding' to reduce protein fouling.[10] Typically, materials with a PEG coating are taken up in a non-specific way, showing little binding to surface proteins, and have an increased circulation time *in vivo,* thus can be used effectively as a comparison to glyco-nanoparticles.

A common method used for studying particle binding to surface proteins, and in particular lectins, is UV-Vis turbidimetric analysis with a multivalent lectin such as Concanavalin A (Con A).[11] Typically in these studies a simple absorbance reading is taken over time after mixing a particle with a lectin, an increase in absorbance represents a corresponding binding between the two. Whilst this technique is quick and easy to perform, the absorbance readings are affected by the light scattering effect of nanoparticles and the dilution effect displayed when further solution is added to a reaction. Other techniques to determine lectin-particle binding, including aggregate size analysis using DLS, have widely been used in determining thermal stability of metal nanoparticles, but much less widely used for studying polymer particle-lectin aggregation.[12-20] Online aggregate size analysis represents an interesting way of tracking lectin-particle aggregation as it will not be adversely affected by particle light scattering or by dilution. The aggregate size analysis is, however, limited to the limits of DLS, where the aggregate must remain small enough for Brownian forces to dominate gravitational force, preventing sedimentation, which for polymeric particles is generally considered to be 500nm.[11] Consequently, to use DLS to track aggregation, polymeric particles must be synthesised with a narrow size distribution well below 500 nm in diameter.

Traditional emulsion polymerisation provides a facile method to generate polymeric nanoparticles, with narrow size distributions and is routinely used in industry for polymer synthesis at scale.[21] Typically

these polymer particles show poor biocompatibility, hence controlled radical polymerisation (CRP) methods are now being utilised to generate functional latex particles[22] CRP methods are becoming increasingly relevant in the synthesis of new bio-applicable materials[23], not only due to their ability to control molar mass, but also the control over the architecture and end-group functionality. Translation of CRP methods into emulsion polymerisation has yielded multiple approaches utilizing various techniques.[24] One strategy utilises amphiphilic macromolecular reversible addition fragmentation chain transfer (macro-RAFT) agents, which form polymeric micelles in aqueous solutions. These are subsequently chain extended during an emulsion polymerisation, yielding polymeric nanoparticles, decorated with the hydrophilic section of the initial macro-RAFT agent. Since its conception by Hawkett and co-workers,[25] there have been relatively few reports of this technique to generate nanoparticles for bio-applications, and have mostly focused on mechanistic studies or using this approach to push the limit of polymer synthesis.[26-30] However, in 2010, Stenzel and co-workers reported the synthesis of glucose functionalised polystyrene nanoparticles via an *ab initio* RAFT emulsion polymerisation, from a glucose based amphiphilic macro-RAFT agent, and their subsequent binding to Concanavalin A and E.coli.[31] Additionally, Ladmiral and co-workers described the synthesis of galactose functionalised nano-objects using RAFT mediated polymerisation-induced self-assembly, and showed intracellular delivery of rhodamine B octadecyl ester.[32] Our group recently reported the synthesis of polyacrylamide stabilised polystyrene nanoparticles, synthesised using RAFT emulsion polymerisation, and their subsequent loading and release of MicroRNA via a redox responsive linker.[33] RAFT emulsion offers a facile, scalable process for the preparation of core-shell nanoparticles, whilst also utilising the versatility of RAFT polymerisation for applications in a wide range of areas.

Herein we describe the synthesis and characterisation of well-defined mannosylated and PEGylated nanoparticles, with discrete size control. The synthesised particles are used to precisely probe the effect of particle size on lectin binding, as well as comparing mannosylated nanoparticles to PEGylated particles, using the commonly used UV-Vis turbidimetric analysis, and an analytical approach based on an online DLS aggregation tracking system, which use is reported here for the first time.

**2. Results and Discussion**

Mannose Acrylamide monomer synthesis

Initially, a mannose containing monomer was synthesised using a modified method reported by Cameron and co-workers.[34] This approach utilised boron trifluoride diethyl etherate as an activating agent to induce neighbouring group participation and subsequent nucleophilic substitution of a α-D-Mannose pentaacetate at the anomeric carbon with a hydroxyethyl acrylamide.[35, 36] Advantageously this method results in a preference for the required biologically active α-anomer, thus following deprotection and subsequent column chromatography, yielded mannose acrylamide (ManAm) in c.60% yield with high α-stereospecificity. The monomer was stored with protection from light at -20°C in a freezer, preventing autopolymerisation.
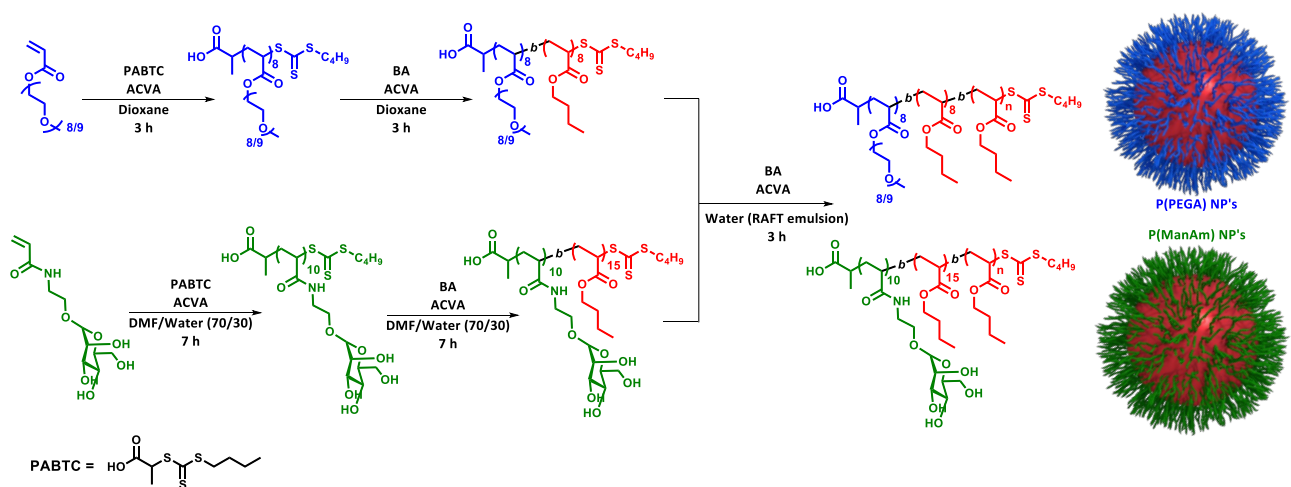
Figure 1 Stepwise synthetic scheme of P(PEGA) and P(ManAm) macro-RAFT agents and subsequent particle synthesis *via* RAFT emulsion polymerisation.

Macro-RAFT agent synthesis

Previous literature regarding RAFT emulsion polymerisation indicates that short chain oligomers act as sufficient stabilisers for the formation of particle.[37] Hence, both: P(ManAm)-*b*-P(BA) and P(PEGA)-*b*-P(BA) were synthesised with butyl acrylate blocks of less than 20 monomer units,.

Polymerisation of the ManAm block was conducted in a DMF/Water mixture (70/30 v/v) at 70°C for 7 h mediated by chain transfer agent PABTC using thermal initiator ACVA as a radical source with >99% monomer conversion confirmed by ^{1}H NMR spectroscopy. PABTC has previously been shown to be an excellent RAFT agent for both acrylate[38] and acrylamide monomers.[39] In addition to this, the negatively charged carboxylic acid moiety on the R group may induce electrostatic stabilisation of the

114   resulting nanoparticles, enhancing the steric stabilisation provided by the hydrophilic polymer, thus

115   increasing the colloidal stability of any final latex particle. After the first block had reached complete

116   monomer conversion, only 43% of the initiator had been consumed,[40] therefore polymerisation of the

117   hydrophobic block was performed without purification. The required amount of *n*-butyl acrylate was

118   then injected into the above reaction mixture without additional initiator, and heated for a further 7 h

119   reaching 97% monomer conversion. Following ^{1}H NMR analysis, it was deduced that overall structure

120   of the mannose di-block copolymer was P(ManAm)$_{10}$-*b*-P(BA)$_{15}$ by comparing ^{1}H NMR signals for side

121   chain protons and protons on the RAFT end group (Supporting information Figure S2). DMF SEC

122   analysis showed a monomodal chromatogram of M_n = 4600 g mol^{-1} and $Đ$ = 1.13 (Supporting

123   information Figure S3). Due to the amphiphilic nature of the macro-RAFT agent, and subsequent

124   polymers, solubility in common SEC solvents was low, producing a poor baseline due to low intensity

125   signal. However data that was collected is shown for completeness.

126

127   Polymerisation of PEGA was conducted at 70°C mediated by PABTC in 1,4-dioxane with ACVA as a

128   thermal initiator. In order to maintain a high livingness, the polymerisation was stopped after 3 h

129   resulting in 21% initiator and 91% monomer consumption. The residual monomer was removed with

130   precipitation in a mixture of hexane and diethyl ether prior to polymerisation of the next block. For the

131   hydrophobic section the P(PEGA) macro-RAFT was chain extended with of *n*-BA over 3 h at 70°C

132   reaching 96% monomer conversion. Both blocks had monomodal symmetrical SEC chromatograms and

133   narrow dispersity ($Đ$ = 1.13) with a clear shift to higher molar mass upon chain extension. ^{1}H NMR

134   analysis indicated that the resulting block copolymer had the structure P(PEGA)$_8$-*b*-P(BA)$_8$ which was

135   in good agreement with experimental molar mass determination with SEC (Supporting information

136   Figure S6). For a general overview of the synthesis see Figure 1.

137

138   To confirm that both ManAm and P(PEGA) macro-RAFT agents would be suitable stabilisers, their

139   self-assembly in aqueous solution was investigated. DLS measurements were performed at 15 mg mL^{-1}

140   and, as such, displayed mean diameters of 10 and 7 nm for ManAm and P(PEGA) block co-polymers,

141   respectively. Micelles formed for both block copolymers had low PDi values of 0.06 suggesting that

142   both types of micelle were uniform, likely due to the stability received from the negative ζ-potential

143   caused by the deprotonated carboxylic acid from the R group of the macro-RAFT agents (see Table 1

144   for characterisation).

145

146   ***Nanoparticle Synthesis***

147   The conditions used for the RAFT emulsion polymerisation of n-BA mediated by $P(ManAm)_8$-$P(BA)_{15}$

148   and $P(PEGA)_8$-$P(BA)_8$, were adapted from literature conditions (see Figure 1).[33] Oxygen was

149   removed from the polymerisation mixture by purging with N_2 gas in a vial sealed with a septum, the

150   monomer was degassed in a separate vial, and transferred into the micelle solution using a gas-tight

151   syringe, to avoid monomer evaporation and improve the reproducibility of the polymerisation. Multiple

152   emulsion polymerisations were performed, each with modification of [M]/[CTA] resulting in

153   monodisperse latex particles (PDi <0.1) with diameters ranging from 82 to 176 nm for nanopaticles with

154   P(ManAm), and 29 to 119 nm for nanoparticles P(PEGA) shells (Table 1). ^{1}H NMR samples were

155   prepared by diluting 100 µL of latex in either d_6-acetone or an 80/20 (v:v) mixture of d_6-DMSO for

156   P(PEGA) nanoparticles and P(ManAm) nanoparticles respectively. Interestingly, for polymerisations

157   with identical DP_{target} for both P(PEGA) and P(ManAm) RAFT emulsion polymerisations, P(ManAm)

158   particles had a significantly larger diameter compared to their respective P(PEGA) particles (Table 1).

159   For example when a chain extension of 100 monomer units was targeted it was observed that P(PEGA)

160   particles had mean diameters of 50 nm whereas P(ManAm) particles were 90 nm. This finding has been

161   attributed to a decreased stabilization of the P(ManAm) macro-RAFT agent during the RAFT emulsion

162   polymerisation since the P(PEGA) macro-RAFT agent consists of a highly hydrophilic polymer brush

163   block, compared to a linear polymer block for the P(ManAm) macro-RAFT agent. Similar to the block

164   copolymer micelles, the resulting nanoparticles had negative ζ-potential due to the carboxylic acid end

165   groups. Values ranged from -20 mV to -47 mV for P(PEGA) nanoparticles depending on size, however

166   P(ManAm) nanoparticles had ζ-potential consistently close to -32 mV. To measure the molecular

167   weight distribution of a single polymer chain, the nanoparticles were disassembled either by drying and

168   subsequent dissolution in chloroform or THF, or simply adding an excess of THF or DMF, for

169   P(PEGA) and P(ManAm) nanoparticles respectively. SEC chromatograms of the polymeric unimer for

170   P(PEGA) nanoparticles show three populations: firstly a low molecular weight distribution

171   corresponding to unconsumed macro-RAFT agent, also observed by Rieger and co-workers for RAFT

172   emulsion polymerisation of n-BA[41]; second, a population indicative of successful chain extension in

173   the emulsion polymerisation which shows good agreement with $M_{n,th}$; and third a high molecular weight

174   shoulder due to termination and/or mid-chain branching typical for acrylate polymerisation. If the

175   population relating to unconsumed macro-RAFT agent is ignored the Đ values remain below 1.4 for all

176   particles. It is expected that this unconsumed macro-RAFT agent is associated at the particle water

177   interface, as other size distributions relating to macro-RAFT agent micelles in DLS measurements were

178   not observed. Additionally, a near linear trend between the theoretical molecular weight of the single

179   polymer chains, and the resulting particle volume for both PEG and mannose shielded latex particles is

seen (Figure 2). This correlation, which can predict the resulting nanoparticle size based on the conditions of the polymerisation allows to increase reproducibility for the synthesis of nanoparticles, which is beneficial for biological applications.
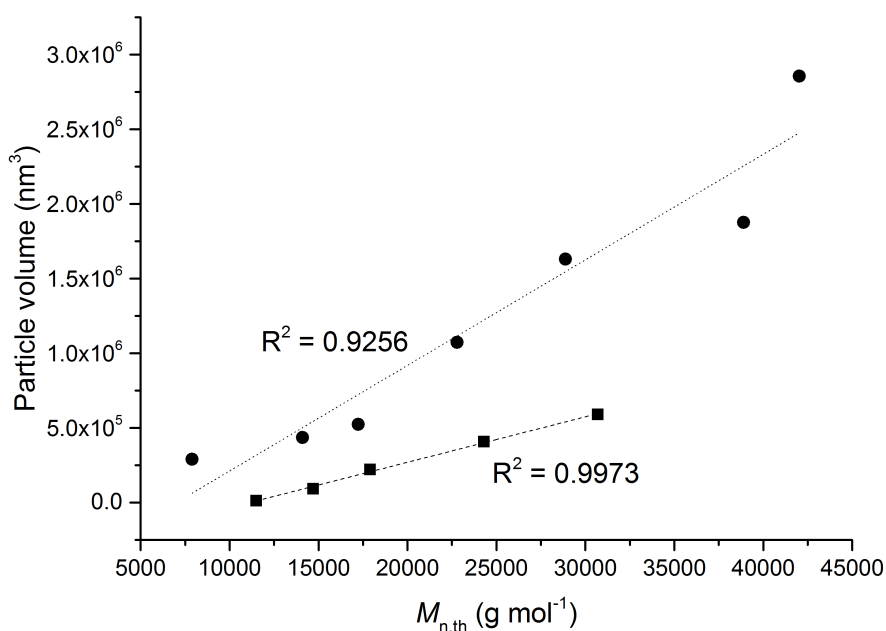
Figure 2. Linear trend between $M_{n,th}$ of a single polymer arm, and the nanoparticle volume. ManAm nanoparticles (circles), PEG nanoparticles (squares)

		$[M]_0/[CTA]_0$	Average Particle Diameter (nm)[a]	PDi[b]	ζ-Potential (mV)	Conversion (%)	$M_{n,SEC}$	Đ[f]
	P(ManAm)$_{10}$-*b*-P(BA)$_{15}$	N/A	11	0.060	-20.	97	4600[c]	1.13
A	P(ManAm)$_{10}$-*b*-P(BA)$_{15}$-*b*-P(BA)$_{25}$	25	82	0.084	-36	99	16000[c]	1.22
B	P(ManAm)$_{10}$-*b*-P(BA)$_{15}$-*b*-P(BA)$_{75}$	75	94	0.085	-34	98	11000[c]	1.33
C	P(ManAm)$_{10}$-*b*-P(BA)$_{15}$-*b*-P(BA)$_{100}$	100	100	0.088	-33	98	13000[c]	1.19
D	P(ManAm)$_{10}$-*b*-P(BA)$_{15}$-*b*-P(BA)$_{154}$	154	127	0.082	-35	93	22000[c]	1.55
E	P(ManAm)$_{10}$-*b*-P(BA)$_{15}$-*b*-P(BA)$_{200}$	200	146	0.13	-32	95	49000[c]	1.63
F	P(ManAm)$_{10}$-*b*-P(BA)$_{15}$-*b*-P(BA)$_{300}$	300	153	0.073	-33	90	41000[c]	1.54
G	P(ManAm)$_{10}$-*b*-P(BA)$_{15}$-*b*-P(BA)$_{400}$	400	176	0.10	-33	75	61000[c]	1.99
	P(PEGA)$_8$-*b*-P(BA)$_8$	N/A	7	0.060	-10	96	6250[d]	1.13
	P(PEGA)$_8$-*b*-P(BA)$_8$-*b*-P(BA)$_{50}$	50	29	0.064	-20	>99	11500[e]	1.22
	P(PEGA)$_8$-*b*-P(BA)$_8$-*b*-P(BA)$_{75}$	75	50	0.078	-37	>99	14200[e]	1.35
	P(PEGA)$_8$-*b*-P(BA)$_8$-*b*-P(BA)$_{100}$	100	75	0.058	-36	>99	18400[e]	1.39
	P(PEGA)$_8$-*b*-P(BA)$_8$-*b*-P(BA)$_{150}$	150	93	0.060	-46	>99	22500[e]	1.60
H	P(PEGA)$_8$-*b*-P(BA)$_8$-*b*-P(BA)$_{200}$	200	130	0.050	-46	>99	25700[e]	1.86

188 **Table 1.** Characterisation of nanoparticles and their individual polymer arms synthesised with RAFT emulsion
189 polymerisation. [a]Determined by DLS (number distribution),[b]PDi values calculated using equation S1 (see supplementary
190 information), [c]Determined by DMF-SEC analysis with PMMA standards, [d]Determined by THF-SEC analysis with PMMA
191 standards, [e]Determined by CHCl$_3$-SEC analysis with PMMA standards.[f]Dispersity values are for all populations in
192 chromatogram, i.e not omitting any unconsumed macro-RAFT agent.

193

194 ***Aggregation Studies***

195 Having synthesised a range of well-defined nanoparticles with PEG and mannose shells, these could be
196 used in lectin binding aggregation studies. Investigations into the lectin binding of glyco-nanoparticles
197 typically heavily relies on the use of UV-Vis turbidimetry, which allows particle aggregation to be
198 tracked in real time in a straight forward manner.[11, 42] Turbidimetry is, however, affected by light
199 scattering of nanoparticles, the dilution effect upon solution addition, and provides limited information
200 regarding the particle binding and aggregation mechanism. By tracking aggregation online with DLS,
201 these issues can be overcome, and more information regarding the composition of aggregates and the
202 mechanism by which they form may be obtained. Similar techniques have previously been used, more
203 commonly to measure aggregation of metal nanoparticles (e.g. iron), with only a few examples for
204 measuring polymer particle-lectin aggregation.[12, 14, 16, 18, 19] In order to evaluate the potential of
205 DLS as a technique to study the lectin binding of nanoparticles, both DLS and turbidimetry were used
206 and compared.

207 ***Method Optimisation***

208 Before attempting an in-depth study it was necessary to optimize conditions for UV-Vis aggregation
209 experiments such that they could be transferred to DLS measurements without modification. In typical
210 UV-Vis lectin binding turbidimetric experiments, the particle solution is added to the lectin solution.
211 However, given the high viscosity of certain particle solutions that lead to blockage of the cannula, a
212 more reliable approach was to inject the Con A solution into the particle solution. DLS measurements
213 must also be conducted without stirring or agitation due to the inherent Brownian motion of the particles
214 to calculate particle size. In order to assess if these prerequisites affect measurements, effect of stirring
215 and the order of addition (Con A to particles, or particles to Con A) on the aggregation was investigated,
216 using 82 nm P(ManAm) particles as models (Figure 3).

217
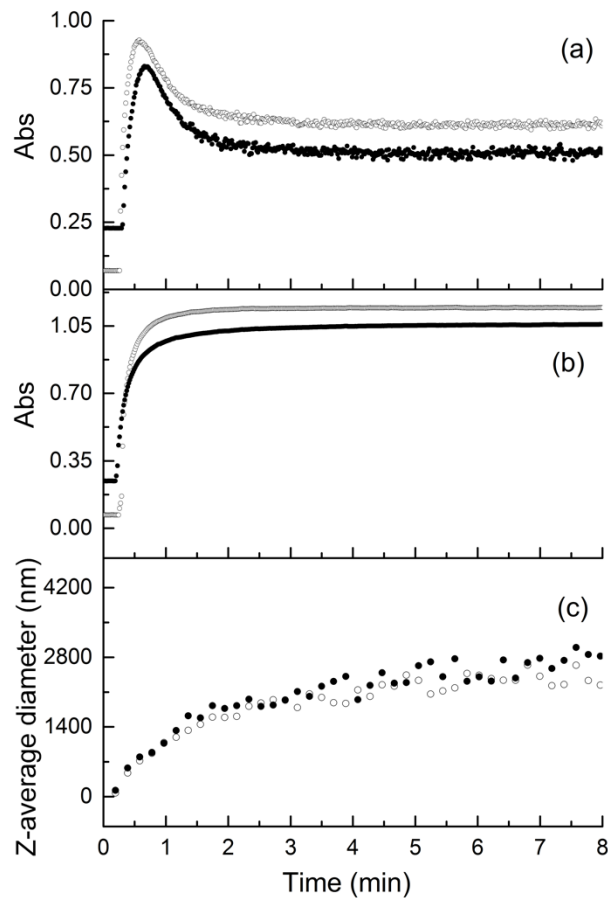
Figure 3. Effect of stirring and order of addition. (a) stirring UV-Vis (b) not stirring UV-Vis (c) not stirring DLS. Particle solution into Con A solution (hollow circles), Con A solution into particle solution (filled circles)

The order of addition showed little effect on final particle size in the DLS measurements and a negligible effect on final turbidity or trace shape in the UV-Vis results. There is a small increase in binding time when particles are added to Con A, which may be attributed to a slower diffusion of particles through Con A solution than Con A through particle solution (Figure 3(c)). The effect of stirring is, however, far more pronounced, seen in the UV-Vis traces (Figure 3(a)). For both sets of experiments (with and without stirring) an initial sharp increase in absorbance was detected, related to the aggregation between particles and Con A. In the absence of stirring, the absorbance plateaus to a value between 0.8-1 (Figure 3(b)), however, the solutions, which were being stirred, showed a subsequent decrease in absorbance between 20-100 s, before the absorbance plateaus to a much lower final value of 0.6. A potential explanation for this phenomenon is that stirring increases particle movement and, hence, collision between particles and aggregates, increasing the chance of successful binding interactions between them. This higher rate of successful collisions causes the formation larger aggregates more rapidly than in solutions without stirring. These aggregates become large enough to sediment out of solution, only being kept in suspension by stirring and, ultimately, giving a lower

absorbance value. Further evidence supporting this hypothesis was observed optically, as mixtures, which had been stirred were observed to completely sediment within minutes, whereas not stirred solutions were stable up to 24 h. If the not stirred solutions were subsequently stirred, sedimentation occurred within minutes. Based on these results further experiment were performed by the addition of Con A into particle solution without stirring, allowing the use of DLS in tracking particle aggregation.

UV-Vis studies
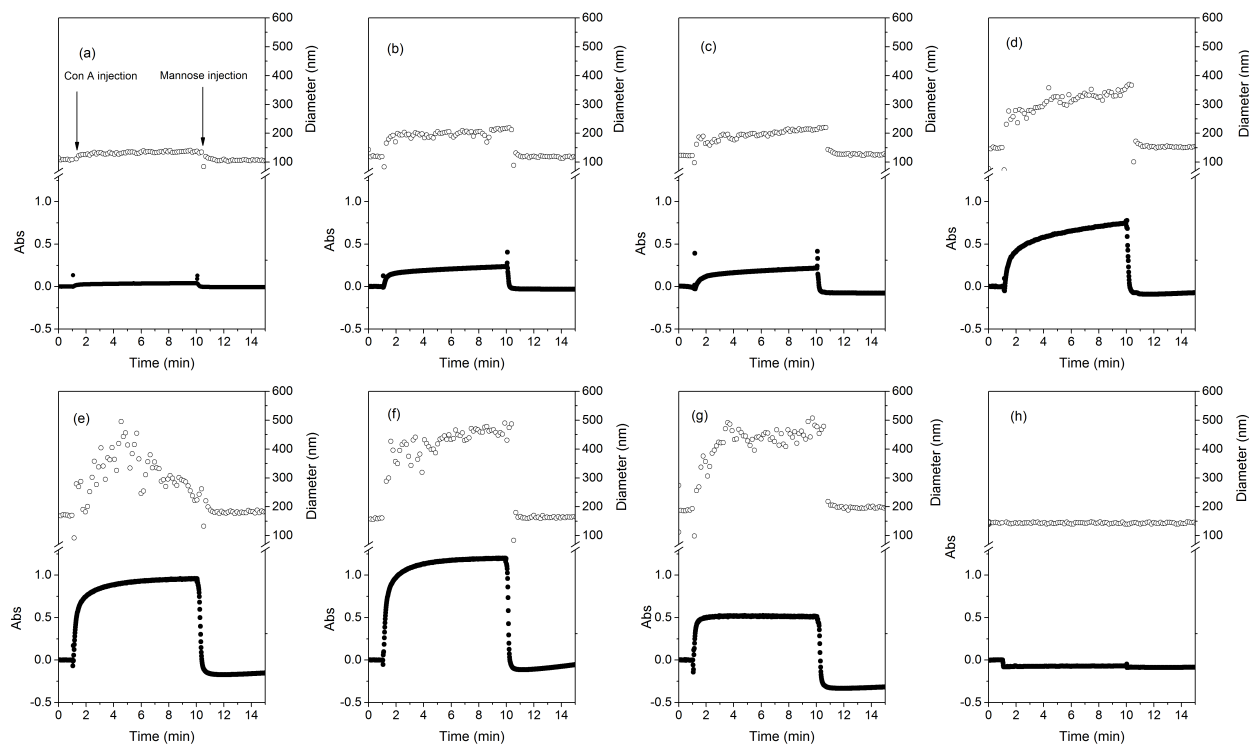
Figure 4. Nanoparticle-lectin aggregation with both turbidimetric (filled circles) and DLS (hollow circles) for P(ManAm) particles (a) 82 nm (b) 94 nm (c) 100 nm (d) 127 nm (e) 146 nm (f) 153 nm (g) 176 nm, and P(PEGA) particle (h) 130 nm. Arrows indicate time of injection for Con A and Mannose solutions.

After optimising test conditions, turbidimetric studies were conducted using UV-Vis spectroscopy, using PEG and ManAm coated particles across a variety of sizes. To conduct these measurements, a cuvette was placed in the machine loaded with the requisite nanoparticle solution and an absorbance reading was taken every second at 500 nm. After 60 s the Con A solution was added and immediately after the addition a sharp increase in absorbance was observed in all of the particles coated in ManAm, followed by a plateau in absorbance after a further 2 min. No response was detected for measurements using particles with a PEGA shell, confirming that the aggregation shown is due to lectin sugar

257   interaction between Con A and Mannose residues on the ManAm coated particles. After 10 min, an
258   excess of α-D-mannose was injected, causing a sharp drop in absorbance to below the original baseline
259   for all of the ManAm particles. This shows a reversible, non-covalent binding mechanism between Con
260   A and the mannose residues. The only response seen for PEG particles was a reduction in absorbance
261   due to the dilution cause by mannose addition, reducing the overall concentration of particles (Figure 4).
262   The results indicate that with increasing ManAm particle size a corresponding increase in the maximum
263   absorbance observed. The influence of the aggregate composition can, however, not be inferred from
264   this data , as the relationship between size and light scattering (Rayleigh scattering relationship) is non-
265   linear.[43] To investigate the aggregation and the formed aggregates further, a different technique is
266   required. Online DLS measurements present a suitable way of obtaining this information.

267

268   ***DLS Studies***

269   DLS measurements were performed by mixing Con A and particle solutions within the DLS
270   machine after readings had commenced via a cannula injection system allowing the solutions to be
271   combined without opening the sample chamber. Measurements were taken every 11.6 seconds and
272   addition of Con A to particle solutions occurred after the 6th measurement into the experiment (69.9 s)
273   in all cases. During the experiments at the point of injection, an artificially low diameter is recorded as
274   the mixing causes the particles to move faster in solution than they would based solely on Brownian
275   motion.[44] The experiments were performed at the same concentration and are shown as Z-average
276   diameter over time in Figure 4, (diameter by intensity is shown in supporting information, Figure S11).
277   Particle size distribution by number was used to characterise initial particle size to minimise the
278   influence of any aggregation present, giving the most accurate representation of particle diameter.
279   Conversely, to determine the most accurate final aggregate size, the influence of free particles on the
280   measurement needed to be minimised, for this reason size distribution by intensity was used here.

281

282   All ManAm coated particles showed an initial increase in Z-average diameter upon the addition of Con
283   A due to aggregation, which then plateaus. Again no response is observed for PEG particles, confirming
284   that the mannose residues are solely interacting with Con A, while also confirming that the presence of
285   Con A does not cause any major discrepancy to size measurements using DLS. Similar to UV-Vis
286   experiments a solution of α-D-mannose was injected, leading to a sharp decrease in Z-average diameter
287   corresponding to the original particle diameter detected at the start of the experiment. No change in PEG
288   particle Z-Average diameter is seen on the addition of either Con A or α-D-mannose solutions, further
289   confirming that no dilution effect needs to be taken into account, when using DLS to measure

aggregation. The results presented to this point are broadly in agreement with the absorbance results obtained for UV-Vis. However, using the data collected from the online DLS aggregation experiments it is possible to obtain further information compared to UV-Vis. Firstly, after the Z-average diameter increased and plateaued, a drift to larger diameter was observed for smaller particles (Figure 4). This slow increase in apparent diameter is attributed to aggregation occurring in two distinct phases: Initially a fast aggregation with a high concentration of free Con A and particles forming initial aggregates, followed by secondary agglomeration between formed aggregates, slowly interacting with each other (and any free particles and Con A in solution), to slowly grow in size. Due to the nature of Rayleigh light scattering in turbidimetric measurements, the initial phase of aggregation shows as a very large increase in absorbance. This further growth in already formed aggregates will only produce a comparably small change in absorbance, making it difficult to determine. This relationship was observed when the DLS and UV-Vis data is plotted together, with Z-average diameter on a $\log_{10}$ scale and absorbance on a linear scale (Supporting information Figure S10). In this plot the two traces overlap, suggesting that UV-Vis data alone, provides artificially short aggregation time. and that any small aggregate growth after the initial increase would be difficult to determine.

Initial Particle Diameter (nm)[a]	Initial Particle Volume (nm^3)	Aggregate Diameter by Intensity (nm)[a]	Aggregate Vol (nm^3)[b]	N_{agg}	$N_{agg,th}$
82	290,000	138	1,400,000	1.52	5.52
94	430,000	206	4,600,000	1.97	4.81
100	520,000	214	5,100,000	1.9	4.52
127	1,100,000	390	31,000,000	2.81	3.56
146	1,600,000	496	64,000,000	3.07	3.1
153	1,900,000	589	107,000,000	3.55	2.96
176	2,900,000	591	108,000,000	3.03	2.57

Table 2. Analysis of final aggregate diameters compared to initial particle diameter. [a]Measured by DLS, [b]determined using aggregate diameter by intensity and formula for the volume of a sphere.

By using DLS, an estimation of aggregate volume can be made by using the final aggregate radius in the formula for the volume of a sphere. The cubed root of the aggregate volume, divided by the initial volume of the particles forming the aggregate, and multiplied by the ideal packing number of spheres (74%), gives an estimate of the aggregation number as particles per aggregate (ppa) formed.[45] This information can further be used by comparing it to the theoretical maximum number of aggregation at a diameter of 500 nm. This diameter marks the particle size limit for Brownian motion to overcome gravity and as such, the point at which sedimentation will occur, these results are shown in Table 2.[11]

The values for aggregate diameter were obtained by taking an average diameter (by intensity) after the initial phase of aggregation had finished. A clear increase in aggregate size can be seen as the initial particle diameter becomes larger, this of course, could simply be due to the aggregates being composed of larger particles. However, by determining the number of particles needed to compose each aggregate, an increase in aggregation number can be seen from 1.25 ppa for 82 nm diameter particles, to 2.85 ppa for particles 153 nm in diameter. Data for the largest two particles (153 and 176 nm) is, however, unreliable due to high dispersity and large aggregate size. Looking at the relationship between number of aggregation for each particle and the theoretical maximum number of aggregation, it can be seen that as the initial particle diameter increases, the observed number of aggregation approaches the theoretical maximum, until it is exceeded by the two largest particles. This further confirms the hypothesis that the DLS data for particles of diameter 153 and 176 nm is unreliable, and that an aggregate size of 500 nm represents an upper size limit for DLS to determine.

It is hypothesised that the increasing number of aggregation observed as particle diameter increases is related to the increased surface area of the initial particle. Larger particles will have more mannose residues presented on their surface and thus be able to interact with more Con A. In having more Con A associated to the surface of a particle, it is statistically more likely to have a successful binding interaction upon collision with another mannose decorated particle. Furthermore, the contact angle between two particles interfaces decreases with increasing particle size leading to an increased area of interaction with Con A and thus a corresponding increase in possible number of aggregation.

The data presented here shows that by using online DLS measurements particle-lectin binding can provide data equivalent to that produced with a UV-Vis turbidity technique. Whilst turbidimetric measurements are useful as a qualitative measure of aggregation, a definite time for binding cannot be determined. Turbidimetry is also greatly affected by the light scattering ability of particles, and the dilution effect observed upon solution injection. An online DLS measurement however provides the same information but gives a more clear determination of how aggregation is occurring throughout the reaction. In contrast to turbidimetry light scattering of particles has no adverse effects on the measurement. By producing a final aggregate size, a number of aggregation per particle can also be estimated, which represents a robust way of measuring the effect of particle size on aggregation. However, by using DLS an upper size limit of 500 nm for particles and aggregates is introduced, past which data becomes unreliable.

3. Conclusions

In conclusion, the synthesis of short amphiphilic di-block copolymers via RAFT polymerisation has been demonstrated. These macro chain-transfer agents were used to produce a wide range of well-defined polymer particles utilizing RAFT emulsion polymerisation. Particles were stabilised in solution by a shell of P(PEGA) or P(ManAm), respectively, depending on the di-block copolymer used.

Using these particles, lectin binding studies using turbidimetric and online-DLS measurements in the presence of Con A were performed. Increasing particle size has shown to improve lectin binding using both methods. DLS offers a robust, quick and easy technique for particle-lectin aggregation studies and avoids issues of changes in absorbance caused by light scattering as well as dilution factors. Furthermore, the technique enables detailed insight into aggregate formation and composition, valid up to an aggregate diameter of 500 nm. Future studies will focus on the interaction of varied glyco-particles with more bio-applicable lectins.

4. Acknowledgement
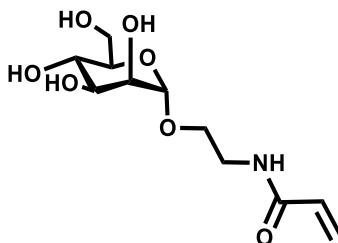
Experimental

Materials and methods

Materials and methods can be found in the supplementary information section.

Synthesis

Mannose Acrylamide[34]

7.5 g (0.0192 mol, 1.13 eq) of α-D-mannose pentaacetate and 2.01 g (0.017 moles, 1eq) of hydroxyl ethyl acrylamide were dissolved in 77 mL of anhydrous DCM in a 250 mL round bottomed flask (RBF) equipped with a magnetic stirrer and an appropriately sized rubber septum. The reaction mixture was

purged with nitrogen gas and 13.33 g of boron trifluoride diethyl etherate (0.044 mol, 11.6 mL) was transferred using a gas-tight Hamilton syringe charged with nitrogen. The reaction mixture was consequently subjected to four cycles of 10 min sonication and 5 min rest prior to stirring at ambient temperature for 48 h. The progress of the reaction was monitored with thin layer chromatography (TLC) using a 9:1 chloroform:methanol mixture (v/v), and stained with 5% sulfuric acid in ethanol. Once complete the reaction mixture was then diluted with two parts DCM and washed thoroughly three times with brine then water in an appropriately sized separating funnel. The organic phase was dried over magnesium sulfate, filtered *via* vacuum filtration and the solvent removed under reduced pressure at a temperature no higher than 30°C leaving an orange brown viscous liquid. This was dissolved in 40 mL of potassium carbonate in methanol, purged with nitrogen gas and stirred at ambient temperature for 24 h. The pH was adjusted to pH 7 with a Dowex 50WX4 hydrogen form exchange resin and stirred until the pH was fully adjusted. The Dowex resin was removed with vacuum filtration and solvent removed under reduced pressure at a temperature no higher than 30°C. The crude product was purified *via* column chromatography on an 80 g silica column and eluted with a 2:8 methanol: chloroform mixture at a flow rate of 1 mL min^{-1}, on an auto-column equipped with a UV-Vis detector set to 308 nm. The product was found to elute at around 15 min. Product fractions were combined, the solvent evaporated to less than 10 mL under reduced pressure and subsequently freeze dried to yield the pure monomer as a white powder.

^{1}H NMR (D$_2$O, 400 MHz) δ_H: 6.13 (dt, J = 31.0, 13.5 Hz, 2H, **CH$_2$CH**), 5.65 (d, J = 10.0 Hz, 1H, CH$_2$**CH**), 4.74 (s, J = 16.2 Hz, 1H, C**HO$_2$**CH), 3.80 (s, J = 122.4 Hz, 1H, CH$_2$**OH**), 3.76 – 3.28 (m, 9H).
^{13}C NMR (D$_2$O, 400 MHz): δ 129.75 (s) (**CH**CH$_2$), 121.41 (m) (CH$_2$**CH**), 99.61 (s) (**CH$_2$OH**), 72.71 (s) (**CHO**), 70.39 (s) (**CHO**), 69.92 (s) (**CHO**), 66.52 (s) (**CHO**), 65.69 (s) (**CHO**), 60.76 (m) (**CH2O**), 37.77 (m) (**CH$_2$NC**).
MS *m/z* [M+Na]$^+$: 300.1 (MS$_{th}$: 300.9)
IR (cm^{-1}): 3275 (b), 2928 (b), 1656 (n), 1624 (m), 1548 (b), 1409 (m), 1317 (w), 1249 (m), 1131 (m), 1089 (m), 1051 (s), 1023 (s).

2-((((butylthio)carbonothioyl)thio)propanoic acid[25]
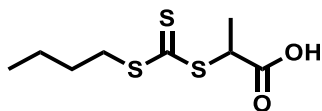
A 50% w/w sodium hydroxide solution (9.68 g NaOH, 0.242 mol, 1.1 eq) in water was added to a mixture of butanethiol (20 g, 0.22 mol, 1 eq) dissolved in acetone (11 mL). Water (40 mL) was added

408   and the solution was stirred for 30 min at room temperature. Carbon disulphide (17.32 g, 0.228 mol,

409   1.025 eq) was added and the orange solution was stirred for 30 minutes at room temperature, then

410   cooled in ice below 10°C. 2- Bromopropionic acid (34.9 g, 0.228 mol, 1.025 eq) was added slowly,

411   monitoring the temperature, and subsequently a further 19.36 g of 50% w/w sodium hydroxide solution

412   was added. The reaction mixture was left to stir for 18 h at ambient temperature. 200 mL of water was

413   added to the reaction mixture, cooled in ice, and a 10 M solution of HCl was added dropwise until the

414   pH reached between 2-3. The resulting precipitate was filtered, washed with water, and recrystallised in

415   hot hexane to afford 36.53 g of 2-(((butylthio)carbonothioyl)thio)propanoic acid. Yield = 70%.

416

417   ^{1}H NMR (400 MHz, CDCl$_3$) δ_H 6.06 (br, 1H, CO$_2$**H**), 4.86 (q, J = 7.4 Hz, 1H, SC**H**), 3.37 (t, J = 7.4 Hz,

418   2H, C**H**$_2$S), 1.69 (quint, J = 7.5 Hz, 2H, C**H**$_2$CH$_2$S), 1.63 (d, J = 7.4 Hz, 3H, SCHC**H**$_3$), 1.43 (sext, J =

419   7.5 Hz, 2H, CH$_3$C**H**$_2$CH$_2$), 0.94 (t, J = 7.3 Hz, 3H, C**H**$_3$CH$_2$).

420   ^{13}C NMR (75 MHz, 298 K CDCl$_3$) δ_c 175.4 (**C**OOH), 47.2 (**S**CH), 37.1(**C**H$_2$S), 29.88 (**C**H$_2$CH$_2$S),

421   22.1(CH$_3$**C**H$_2$CH$_2$), 16.4 (**C**H$_3$CH), 13.6 (**C**H$_3$CH$_2$CH$_2$).

422   FTIR (cm^{-1}): 3093, 2958, 2929, 2871, 2362, 2340, 1454, 1412, 1285, 1230, 1200, 1089, 1059, 912, 861.

423   MS (ESI) m/z 237.0 [M-H], 238 [M-]

424

425   **Poly(Mannose Acrylamide)$_{10}$-poly-*n*-(butyl acrylate)$_{15}$ synthesis**
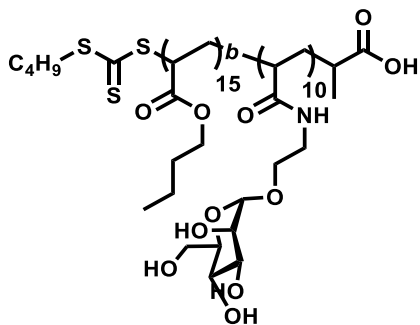
426

427   Mannose acrylamide (1g, 3.62 mmol), 2-((butylthio) carbonothioyl) thio)propanoic acid (PABTC)

428   (0.0864 g, 3.62x10^{-4} mol), and 4,4'-Azobis (4-cyanovaleric acid) (ACVA) (from a pre-made stock

429   solution of 10mg mL^{-1} in DMF:water (70:30) mix) (0.0508 g, 1.81x10^{-4} mol) were dissolved in a

430   mixture of DMF:water (70:30) to a total volume of 10.8 mL in a 25 mL round bottomed flask with a

431   magnetic stirrer bar. The flask was sealed with an appropriate rubber septum and purged of oxygen with

432   nitrogen gas for ten minutes before immersing it into a preheated oil bath at 70°C and stirred for seven

433   hours. Monomer conversion was determined by ^{1}H NMR spectroscopy in D$_2$O, by comparison of the

434   ratio of vinyl peak (δ=6.08) and RAFT agent CH3 z-group butyl chain end group peak (δ=0.78). The

435   polymer was analysed by SEC with a DMF eluent at 30°C ($M_{n\ SEC}$=2450 g mol^{-1} $Đ$=1.27). To chain

extend the synthesised P(ManAm)$_{10}$ macro-RAFT agent, *n*-butyl acrylate was purged of oxygen with nitrogen for ten minutes, and 1.3g (1.01x10^{-2} mol, 1.45 mL) was injected into the 25mL round bottomed flask using a dry Hamilton syringe, purged with nitrogen. The round bottomed flask was then immersed in an oil bath set to 70°C and stirred for seven hours. Monomer conversion was determined by ^{1}H NMR spectroscopy in d_6-DMSO, by comparison of the ratio of vinyl peak (δ=5.94) and RAFT agent CH3 z-group butyl chain end group peak (δ=0.83). The polymer was analysed by SEC with a DMF eluent at 30°C.

P(PEGA)$_8$-*b*-P(BA)$_8$ Synthesis
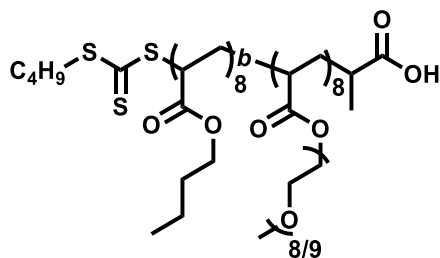
PABTC (0.31 g, 1.30 x 10^{-3} mol), PEGA (5 g, 10.4 x 10^{-3} mol) and ACVA (from a pre-made stock solution in 1,4-dioxane) (18 mg, 6.51 x 10^{-5} mol) were dissolved in 4.9 mL 1,4-dioxane in a 25 mL round bottom flask equipped with a magnetic stirrer bar. The solution was fitted with an appropriate sized rubber septum, and purged with nitrogen for 20 minutes. The round bottom flask was subsequently immersed in an oil bath preheated to 70°C and stirred for 3 h. The reaction vessel was cooled to ambient temperature and opened to oxygen to quench further polymerisation. The pre-cursor polymer was precipitated into a mixture of 20% hexane and 80% diethyl ether (v/v), collected by dissolving in 10 mL of 1,4-dioxane, and the precipitation repeated once more. Finally, the precipitated polymer was dissolved into DCM, transferred to a 20 mL vial, the DCM evaporated and dried in a vacuum oven overnight at 40°C to yield P(PEGA)$_8$ as a yellow viscous liquid (4.5 g). For the second stage of the polymerisation, *n*-butyl acrylate (0.9 g, 7.03 x 10^{-3} mol) and ACVA (from a pre-made stock solution in 1,4-dioxane) (12.3 mg, 4.36 x 10^{-5} mol) were added to 3.58 g of P(PEGA)$_8$ dissolved in 5.92 mL of 1,4-dioxane in a 10 mL round bottom flask. The polymerisation mixture was purged with nitrogen for 20 minutes and heated to 70°C for 3 h. The resulting polymer solution was cooled to room temperature and subsequently purified by precipitation in ice-cold hexane. The yellow viscous liquid was re-dissolved in dichloromethane and the precipitation was repeated once more. Finally, the solvent

465   was evaporated under reduced pressure to yield the di-block macro-RAFT agent as a yellow viscous

466   liquid (3.5 g).

467

468

469

470   ***General method for RAFT-mediated emulsion polymerisation***

471   Nanoparticles of different sizes were prepared by altering the ratio of di-block macro-RAFT agent to

472   monomer in an emulsion polymerisation. As an example P(ManAm)$_{10}$-*b*-P(BA)$_{15}$-*b*-P(BA)$_{400}$ was

473   prepared as follows. NaOH (14.3 mg, 3.6 x 10^{-4} mol) was added to a suspension of ACVA (50 mg, 1.8 x

474   10^{-4} mol) in water (10 mL) to ensure full solubility. P(ManAm)$_{10}$-*b*-P(BA)$_{15}$ (0.015 g, 3.13 x 10^{-6} mol)

475   was dissolved in 0.645 mL of water, in a 2 mL vial fitted with a cap incorporating a rubber septum and

476   equipped with an appropriate magnetic stirrer. 0.175 mL of the above ACVA stock solution was added,

477   and the solution was deoxygenated with nitrogen gas for 20 minutes. *n*-BA (0.160 g, 1.25 x10^{-3} mol)

478   was separately deoxygenated in a vial for 10 minutes. The macro-RAFT agent solution was immersed in

479   a 70°C oil bath, the deoxygenated *n*-BA was injected immediately and the RAFT emulsion

480   polymerisation was stirred for 3 h at 70°C at 400 RPM. After approx. 10 min, the emulsion turned a

481   milky white as the polymerisation proceeded. P(PEGA) mediated RAFT emulsion polymerisations were

482   performed at ten folder higher scale in an identical manner.

483

484   ***General method for UV-Vis aggregation studies***

485   Turbidimetric studies were conducted by diluting 12.5 μL of undiluted particle solution with 1.3 mL of

486   10 mM phosphate buffer in a 4.5 mL polystyrene cuvette, and placed in the UV-Vis spectrometer. In a

487   separate 4.5 mL polystyrene cuvette a stock solution of 2.027x10^{-5} M Concanavalin A in 10 mM

488   phosphate buffer was prepared for use with P(ManAm) and poly (PEGA) particles. Absorbance

489   readings were taken every second at 500 nm, with 185.5 μL of Con A stock solution being added after

490   60 s at which point the lid of the spectrometer opened, 250 μL of Con A in phosphate buffer (2.027x10^{-5}

491   M) was added with an Eppendorf pipette, mixed twice and to induce aggregation. After a further 9 min,

492   50 μL of mannose in phosphate buffer (375 mg mL^{-1}) was added with an Eppendorf pipette and mixed

493   twice to induce competitive binding with the glycosylated nanoparticles. The absorbance was monitored

494   for a further 10 min. Readings were taken using an Agilent Carey 60 UV-Vis machine with Agilent

495   software and analysed using Origin.

496

497   ***DLS Aggregation***

DLS measurements were taken using a Malvern instruments Zetasizer Nano at 25°C with a 4 mW He-Ne 633 nm laser at a scattering angle of 173° (back scattering). For P(ManAm) particle DLS aggregation studies, 12.5 μL of particle solution was diluted with 1.2375 mL of 10 mM phosphate buffer to make a total of 1.25 mL in a 4.5 mL polystyrene cuvette. The cuvette was fitted with a size 23 septum, which was pierced with a cannula attached to a 250 μL Hamilton glass syringe. The cannula was positioned such that, solution ejected through it would run down the side of the cuvette. This prevented the creation of any air bubbles that may have interfered with measurements. The cuvette was placed into the Zetasizer, and the lid closed with the syringe exiting through a slit at the side of the instrument. In a separate 4.5 mL polystyrene cuvette a stock solution of 2.027×10^{-5} M Concanavalin A in 10 mM phosphate buffer was prepared for use with P(ManAm) particles. The Zetasizer was set to take a size reading every 10 s for 1 h, however a delay of 1.66 s was recorded between each reading, adding 598 s to each hour, for which the results have been amended. After the sixth reading, 250 μL of 2.027×10^{-5} M Concanavalin A stock solution was injected via the cannula giving a final volume of 1.5 mL. The final concentration of Concanavalin A and side chain residue was 3.125×10^{-5} M and 2.608×10^{-4} M respectively. The same technique was then repeated with the addition of 250 μL of 75 mg mL^{-1} mannose in phosphate buffer being injected via the syringe cannula after 10 min (to allow full aggregation).

References

[1] M. Köhn, J.M. Benito, C. Ortiz Mellet, T.K. Lindhorst, J.M. García Fernández, Functional Evaluation of Carbohydrate-Centred Glycoclusters by Enzyme-Linked Lectin Assay: Ligands for Concanavalin A, ChemBioChem 5(6) (2004) 771-777.

[2] Y. Bourne, H. van Tilbeurgh, C. Cambillau, Protein-carbohydrate interactions, Curr. Opin. Struct. Biol. 3(5) (1993) 681-686.

[3] S.-J. Richards, L. Otten, M.I. Gibson, Glycosylated gold nanoparticle libraries for label-free multiplexed lectin biosensing, Journal of Materials Chemistry B (2016).

[4] G. Yilmaz, C.R. Becer, Precision glycopolymers and their interactions with lectins, European Polymer Journal 49(10) (2013) 3046-3051.

[5] L.L. Kiessling, J.E. Gestwicki, L.E. Strong, Synthetic multivalent ligands as probes of signal transduction, Angewandte Chemie International Edition 45(15) (2006) 2348-2368.

[6] G. Yilmaz, C.R. Becer, Glyconanoparticles and their interactions with lectins, Polymer Chemistry 6(31) (2015) 5503-5514.

530   [7] L. Otten, E. Fullam, M.I. Gibson, Discrimination between bacterial species by ratiometric analysis
531   of their carbohydrate binding profile, Mol. BioSyst. 12(2) (2016) 341-344.

532   [8] C. Bies, C.-M. Lehr, J.F. Woodley, Lectin-mediated drug targeting: history and applications,
533   Advanced Drug Delivery Reviews 56(4) (2004) 425-435.

534   [9] K. Knop, R. Hoogenboom, D. Fischer, U.S. Schubert, Poly (ethylene glycol) in drug delivery: pros
535   and cons as well as potential alternatives, Angewandte Chemie International Edition 49(36) (2010)
536   6288-6308.

537   [10] P.d. Pino, B. Pelaz, Q. Zhang, P. Maffre, G.U. Nienhaus, W.J. Parak, Protein corona formation
538   around nanoparticles - from the past to the future, Materials Horizons 1(3) (2014) 301-313.

539   [11] E. Tomaszewska, K. Soliwoda, K. Kadziola, B. Tkacz-Szczesna, G. Celichowski, M. Cichomski,
540   W. Szmaja, J. Grobelny, Detection limits of DLS and UV-Vis spectroscopy in characterization of
541   polydisperse nanoparticles colloids, Journal of Nanomaterials 2013 (2013) 60.

542   [12] A.A. Keller, H. Wang, D. Zhou, H.S. Lenihan, G. Cherr, B.J. Cardinale, R. Miller, Z. Ji, Stability
543   and aggregation of metal oxide nanoparticles in natural aqueous matrices, Environ. Sci. Technol. 44(6)
544   (2010) 1962-1967.

545   [13] Y. Li, V. Lubchenko, P.G. Vekilov, The use of dynamic light scattering and Brownian microscopy
546   to characterize protein aggregation, Rev. Sci. Instrum. 82(5) (2011) 053106.

547   [14] T. Phenrat, N. Saleh, K. Sirk, R.D. Tilton, G.V. Lowry, Aggregation and sedimentation of aqueous
548   nanoscale zerovalent iron dispersions, Environ. Sci. Technol. 41(1) (2007) 284-290.

549   [15] J. Rubin, A. San Miguel, A.S. Bommarius, S.H. Behrens, Correlating Aggregation Kinetics and
550   Stationary Diffusion in Protein– Sodium Salt Systems Observed with Dynamic Light Scattering, The
551   Journal of Physical Chemistry B 114(12) (2010) 4383-4387.

552   [16] G. Trefalt, I. Szilagyi, M. Borkovec, Measuring particle aggregation rates by light scattering, 2013.

553   [17] G. Sánchez-Pomales, T.A. Morris, J.B. Falabella, M.J. Tarlov, R.A. Zangmeister, A lectin-based
554   gold nanoparticle assay for probing glycosylation of glycoproteins, Biotechnol. Bioeng. 109(9) (2012)
555   2240-2249.

556   [18] X. Wang, E. Matei, A.M. Gronenborn, O. Ramström, M. Yan, Direct measurement of
557   glyconanoparticles and lectin interactions by isothermal titration calorimetry, Anal. Chem. 84(10)
558   (2012) 4248-4252.

559   [19] X. Wang, O. Ramström, M. Yan, Dynamic light scattering as an efficient tool to study
560   glyconanoparticle–lectin interactions, Analyst 136(20) (2011) 4174-4178.

561   [20] X. Wang, O. Ramström, M. Yan, Quantitative analysis of multivalent ligand presentation on gold
562   glyconanoparticles and the impact on lectin binding, Anal. Chem. 82(21) (2010) 9082-9089.

563   [21] T. Tadros, Emulsion Polymerization, in: T. Tadros (Ed.), Encyclopedia of Colloid and Interface

564   Science, Springer Berlin Heidelberg, Berlin, Heidelberg, 2013, pp. 414-414.

565   [22] M. Manabe, N. Tatarazako, M. Kinoshita, Uptake, excretion and toxicity of nano-sized latex

566   particles on medaka (Oryzias latipes) embryos and larvae, Aquat. Toxicol. 105(3–4) (2011) 576-581.

567   [23] C. Boyer, V. Bulmus, T.P. Davis, V. Ladmiral, J. Liu, S. Perrier, Bioapplications of RAFT

568   Polymerization, Chemical Reviews 109(11) (2009) 5402-5436.

569   [24] P.B. Zetterlund, S.C. Thickett, S. Perrier, E. Bourgeat-Lami, M. Lansalot, Controlled/Living

570   Radical Polymerization in Dispersed Systems: An Update, Chemical Reviews 115(18) (2015) 9745-

571   9800.

572   [25] C.J. Ferguson, R.J. Hughes, D. Nguyen, B.T. Pham, R.G. Gilbert, A.K. Serelis, C.H. Such, B.S.

573   Hawkett, Ab Initio Emulsion Polymerization by RAFT-Controlled Self-Assembly §, Macromolecules

574   38(6) (2005) 2191-2204.

575   [26] F. Stoffelbach, L. Tibiletti, J. Rieger, B. Charleux, Surfactant-free, controlled/living radical

576   emulsion polymerization in batch conditions using a low molar mass, surface-active reversible addition-

577   fragmentation chain-transfer (RAFT) agent, Macromolecules 41(21) (2008) 7850-7856.

578   [27] J. Rieger, G. Osterwinter, C. Bui, F. Stoffelbach, B. Charleux, Surfactant-free controlled/living

579   radical emulsion (co) polymerization of n-butyl acrylate and methyl methacrylate via RAFT using

580   amphiphilic poly (ethylene oxide)-based trithiocarbonate chain transfer agents, Macromolecules 42(15)

581   (2009) 5518-5525.

582   [28] W. Zhang, F. D'Agosto, O. Boyron, J. Rieger, B. Charleux, One-pot synthesis of poly (methacrylic

583   acid-co-poly (ethylene oxide) methyl ether methacrylate)-b-polystyrene amphiphilic block copolymers

584   and their self-assemblies in water via RAFT-mediated radical emulsion polymerization. A kinetic study,

585   Macromolecules 44(19) (2011) 7584-7593.

586   [29] X. Zhang, S. Boissé, W. Zhang, P. Beaunier, F. D'Agosto, J. Rieger, B. Charleux, Well-defined

587   amphiphilic block copolymers and nano-objects formed in situ via RAFT-mediated aqueous emulsion

588   polymerization, Macromolecules 44(11) (2011) 4149-4158.

589   [30] I. Chaduc, M. Girod, R. Antoine, B. Charleux, F. D'Agosto, M. Lansalot, Batch emulsion

590   polymerization mediated by poly (methacrylic acid) macroRAFT agents: one-pot synthesis of self-

591   stabilized particles, Macromolecules 45(15) (2012) 5881-5893.

592   [31] S.S. Ting, E.H. Min, P.B. Zetterlund, M.H. Stenzel, Controlled/Living ab Initio Emulsion

593   Polymerization via a Glucose RAFT stab: Degradable Cross-Linked Glyco-Particles for Concanavalin

594   A/Fim H Conjugations to Cluster E. coli Bacteria, Macromolecules 43(12) (2010) 5211-5221.

595   [32] V. Ladmiral, M. Semsarilar, I. Canton, S.P. Armes, Polymerization-Induced Self-Assembly of

596   Galactose-Functionalized Biocompatible Diblock Copolymers for Intracellular Delivery, Journal of the

597   American Chemical Society 135(36) (2013) 13574-13581.

598   [33] C.K. Poon, O. Tang, X.-M. Chen, B.T.T. Pham, G. Gody, C.A. Pollock, B.S. Hawkett, S. Perrier,

599   Preparation of Inert Polystyrene Latex Particles as MicroRNA Delivery Vectors by Surfactant-Free

600   RAFT Emulsion Polymerization, Biomacromolecules 17(3) (2016) 965-973.

601   [34] N.R. Cameron, S.G. Spain, J.A. Kingham, S. Weck, L. Albertin, C.A. Barker, G. Battaglia, T.

602   Smart, A. Blanazs, Synthesis of well-defined glycopolymers and some studies of their aqueous solution

603   behaviour, Faraday discussions 139 (2008) 359-368.

604   [35] N.R. Cameron, S.G. Spain, J.A. Kingham, S. Weck, L. Albertin, C.A. Barker, G. Battaglia, T.

605   Smart, A. Blanazs, Synthesis of well-defined glycopolymers and some studies of their aqueous solution

606   behaviour, Faraday Discuss. 139(0) (2008) 359-368.

607   [36] B. Capon, Neighbouring group participation, Quarterly Reviews, Chemical Society 18(1) (1964)

608   45-111.

609   [37] M. Siauw, B.S. Hawkett, S. Perrier, Short chain amphiphilic diblock co-oligomers via RAFT

610   polymerization, Journal of Polymer Science Part A: Polymer Chemistry 50(1) (2012) 187-198.

611   [38] L. Martin, G. Gody, S. Perrier, Preparation of complex multiblock copolymers via aqueous RAFT

612   polymerization at room temperature, Polymer Chemistry 6(27) (2015) 4875-4886.

613   [39] G. Gody, T. Maschmeyer, P.B. Zetterlund, S. Perrier, Pushing the Limit of the RAFT Process:

614   Multiblock Copolymers by One-Pot Rapid Multiple Chain Extensions at Full Monomer Conversion,

615   Macromolecules 47(10) (2014) 3451-3460.

616   [40] G. Gody, T. Maschmeyer, P.B. Zetterlund, S. Perrier, Rapid and quantitative one-pot synthesis of

617   sequence-controlled polymers by radical polymerization, Nature communications 4 (2013) 2505.

618   [41] M. Chenal, L. Bouteiller, J. Rieger, Ab initio RAFT emulsion polymerization of butyl acrylate

619   mediated by poly(acrylic acid) trithiocarbonate, Polymer Chemistry 4(3) (2013) 752-762.

620   [42] S. Amin, G.V. Barnett, J.A. Pathak, C.J. Roberts, P.S. Sarangapani, Protein aggregation, particle

621   formation, characterization & rheology, Curr. Opin. Colloid Interface Sci. 19(5) (2014) 438-449.

622   [43] W. Haiss, N.T. Thanh, J. Aveyard, D.G. Fernig, Determination of size and concentration of gold

623   nanoparticles from UV-vis spectra, Anal. Chem. 79(11) (2007) 4215-4221.

624   [44] A. Einstein, Investigations on the Theory of the Brownian Movement, Courier Corporation1956.

625   [45] S. Torquato, T.M. Truskett, P.G. Debenedetti, Is random close packing of spheres well defined?,

626   Phys. Rev. Lett. 84(10) (2000) 2064.

627